land

MDPI

Article

Fine-Scale Territorial Carbon Budget Accounting and Driver Identification in the Central Guizhou Urban Agglomeration, China

Debin Lu [1,2,3,†], Jiaheng Chen [1,2,†], Zhongyin Wei [4,*], Zhang Shi [1,2] and Feifeng Wang [1,2]

[1] Department of Tourism and Geography, Tongren University, Tongren 554300, China; jgyldb@gztrc.edu.cn (D.L.); jiaheng520@126.com (J.C.); shizh_g@163.com (Z.S.); wangfeifeng2025@163.com (F.W.)
[2] Engineering Research Center of Intelligent Monitoring and Policy Simulation of Mountainous Territorial Space, Higher Education Institutions of Guizhou Province, Tongren 554300, China
[3] School of Public Administration, Guizhou University, Guiyang 550025, China
[4] School of Geography, Geomatics and Planning, Jiangsu Normal University, Xuzhou 221116, China
* Correspondence: weizy@jsnu.edu.cn
† These authors contributed equally to this work.

Abstract

Fine-scale accounting of land use carbon budgets and identification of their driving factors provides an essential scientific basis for constructing green and low-carbon territorial spatial systems. This is of great significance for optimizing territorial spatial structure and promoting low-carbon development in urban agglomerations. Taking the Central Guizhou Urban Agglomeration as the study area, this study employed a composite carbon coefficient method to construct a 30 m × 30 m grid-based carbon budget index and quantitatively assessed carbon budget changes induced by land use transitions from 2000 to 2024. POI data and a quantile regression model were further integrated to analyze the dominant spatial characteristics associated with carbon budgets, and a carbon budget monitoring and early-warning index was developed to delineate risk zones. The results show that: (1) From 2000 to 2024, the total area of land use change reached 0.95×10^4 km^2 in the Central Guizhou Urban Agglomeration, accounting for 17.68% of the total land area, and leading to a net increase of 2.3821 million tons of carbon emissions. This increase was primarily associated with the conversion of cultivated land to construction land, with an accelerated growth rate observed in the later period. (2) The spatial patterns of carbon budgets and carbon emission risk levels exhibit a distinct "core–periphery" structure, with high carbon emission levels concentrated in built-up urban areas and lower levels observed in peripheral ecological land. (3) The expansion of construction land is the dominant contributor to the increase in net carbon emissions; industrial, transportation, and residential spaces exert significant positive driving effects, whereas commercial and service spaces show a negative association. (4) Carbon budget risk zoning based on dominant spatial characteristics identifies Guiyang and Anshun as extremely high-risk areas. The results further suggest that reducing carbon-increment spaces and increasing carbon-reduction spaces may play an important role in territorial carbon budget optimization. The integrated "accounting–driving–monitoring" analytical framework established in this study provides a scientific basis for territorial spatial optimization and carbon emission reduction in mountainous urban agglomerations.

Keywords: land use change; carbon budget; grid-based accounting; Central Guizhou Urban Agglomeration

Check for updates

Academic Editor: Shaojian Wang

Received: 24 February 2026
Revised: 2 April 2026
Accepted: 7 April 2026
Published: 11 April 2026

Copyright: © 2026 by the authors. Licensee MDPI, Basel, Switzerland. This article is an open access article distributed under the terms and conditions of the Creative Commons Attribution (CC BY) license.

1. Introduction

Territorial space constitutes the fundamental arena for carbon source and sink processes, and its utilization directly influences regional carbon emissions and carbon sequestration [1,2]. Therefore, optimizing land use patterns and regulating regional carbon budgets through territorial spatial planning and land use regulation has become an important pathway toward achieving China's "dual-carbon" goals. Urban agglomerations have become the dominant spatial form of China's new-type urbanization [3], forming the principal framework of the national–territorial–spatial structure and playing a critical role in enhancing regional competitiveness and promoting high-quality development [4]. At the same time, they are also key regions where population, industry, and construction activities are highly concentrated and where land use/land cover change (LUCC) is most intense and complex. With the rapid urbanization process, population, industry, and construction activities have continued to concentrate in urban areas, resulting in continuous restructuring of land use patterns and rapid growth in energy consumption. Although cities occupy only about 2% of the global land surface, they contribute nearly 75% of global carbon emissions [5,6], while the proportion in China is even higher, reaching approximately 85% [7]. In particular, urban agglomerations formed around megacities or large metropolitan cores with strong regional driving capacity contribute more than 64% of China's total carbon emissions, making them the principal spatial carriers of carbon emissions [8,9]. Within these agglomerations, land use patterns reshape the structure and functioning of terrestrial ecosystems, thereby directly influencing the spatiotemporal dynamics of regional carbon budgets, particularly the balance between carbon emissions and carbon sequestration under land use transitions [10]. Optimizing land use patterns to reduce carbon emissions has become a key theme of national–territorial–spatial planning [2,11,12]. Therefore, understanding the patterns and spatial associations of carbon budget changes in urban agglomerations from the perspective of LUCC is of great significance for optimizing territorial spatial patterns, promoting regional low-carbon transition, and achieving sustainable development.

Extensive research has been conducted worldwide on territorial carbon budget accounting, and estimation approaches have continuously evolved [13–17]. Currently, the primary methods for assessing carbon budgets include the field inventory method (sample plot-based) [18,19], model-based approaches [20,21], and remote sensing-based estimation methods [22,23]. The field inventory method (sample plot-based) directly measures vegetation and soil carbon stocks at sample plot scales and generally provides high accuracy. However, they are labor-intensive, time-consuming, and often constrained by limited long-term observational data. The extrapolation from sample plots to regional scales introduces substantial uncertainty, particularly in mountainous regions characterized by strong spatial heterogeneity. The model-based approaches can be broadly classified into bookkeeping models and spatially explicit models [21,24]. Bookkeeping models describe changes in vegetation and soil carbon stocks under anthropogenic disturbances and reflect carbon cycle dynamics between terrestrial ecosystems and the atmosphere, driven by land use change. These models have been widely applied to estimate cumulative carbon emissions since the Industrial Revolution, with parameters progressively refined through empirical datasets [25]. Spatial models include empirical models and process-based (mechanistic) models [21]. Empirical models typically establish statistical relationships between carbon fluxes and climatic variables. Although they require fewer parameters and are relatively easy to implement, their estimation accuracy is often limited and associated with considerable uncertainty. Since the 1990s, more complex process-based models, such as CASA, CENTURY, and the BIOME series, have been increasingly adopted, significantly improving estimation accuracy but exhibiting strong regional variability [26–28]. Remote sensing-

based methods utilize remotely sensed data as primary driving variables, often coupled with ecological process models or integrated with statistical regression, machine learning, and deep learning techniques for carbon sequestration estimation [29,30]. Additionally, atmospheric CO_2 column concentration observations from satellite platforms have been used to invert ecosystem carbon fluxes through carbon assimilation approaches [31], representing an emerging technique in terrestrial carbon sink estimation. Despite the availability of kilometer-to-meter-scale remote sensing imagery that supports relatively fine-scale carbon accounting, several limitations remain. First, current methods often lack explicit spatial linkage between quantitative accounting results and specific land parcels, limiting their ability to capture detailed spatiotemporal dynamics. Second, existing approaches struggle to disentangle the process-based mechanisms underlying LUCC-induced carbon budget dynamics, limiting the ability to identify whether increases in net carbon emissions result from declining carbon sinks, intensified carbon sources, or structural shifts between source–sink regimes. Third, carbon density is frequently treated as spatially homogeneous within land use categories, failing to represent intra-class heterogeneity. Therefore, substantial challenges remain in improving accounting precision, spatial representation, and mechanism identification. There is an urgent need to develop more fine-scale and interpretable territorial carbon budget accounting and monitoring frameworks.

In addition, natural topographic conditions and landscape configuration exert strong controls on the spatial morphology and land use structure of urban agglomerations, resulting in pronounced regional differentiation [32–34]. However, existing studies on carbon budgets have largely focused on economically developed or plain-type urban agglomerations, with comparatively limited attention to mountainous urban systems. In particular, the spatial heterogeneity of carbon sources and sinks under complex terrain constraints, as well as their underlying driving mechanisms, remains insufficiently characterized. Limitations in spatial scale matching and process interpretability further constrain current assessments, indicating the need for more systematic investigation of carbon budget dynamics in mountainous urban agglomerations. The Central Guizhou Urban Agglomeration, located in the karst-dominated region of Southwestern China centered on the Guizhou Plateau, represents a typical mountainous urban system characterized by dense conical and tower karst landforms, extensive mountain ranges, pronounced topographic relief, and high spatial fragmentation. Rapid urbanization has resulted in a distinctive spatial configuration in which built-up areas and mountainous landscapes are highly interwoven [35]. Compared with plain-type urban agglomerations, this region faces stronger land resource constraints, greater ecosystem heterogeneity, and more complex interactions between carbon sources and sinks [33]. Mountainous terrain restricts urban expansion and intensifies human–land pressures, while relatively intact native or semi-natural vegetation in mountainous areas functions as an important carbon sink and plays key roles in biogeochemical cycling, hydrological regulation, and climate regulation [36–38]. In the context of China's "dual-carbon" goals, examining carbon budget dynamics in mountainous urban agglomerations is therefore of increasing scientific and practical relevance.

Therefore, this study focuses on the Central Guizhou Urban Agglomeration as a representative mountainous urban agglomeration. Building upon the conventional remote sensing-based carbon density method, a multi-factor correction mechanism was introduced to construct a composite carbon coefficient, thereby improving the representation of carbon budget heterogeneity under different land use transitions. A grid-based carbon budget index, corresponding to individual remote sensing pixels, was developed to systematically characterize the spatiotemporal evolution of carbon budgets induced by land use and land cover change (LUCC) from 2000 to 2024. Furthermore, point of interest (POI) data were integrated to analyze the dominant spatial patterns associated with construction land

expansion and associated carbon budget variations, as well as carbon risk zones. The ultimate objective is to establish a fine-scale carbon budget monitoring framework tailored to mountainous urban agglomerations, thereby providing scientific support for territorial spatial optimization and carbon risk management.

2. Materials and Methods

2.1. Study Area

The Central Guizhou Urban Agglomeration is located in central Guizhou Province, covering a total area of approximately 53,800 km^2. It encompasses 33 counties (cities and districts) within six prefecture-level cities, including Guiyang, Zunyi, Anshun, Bijie, Qiandongnan, and Qiannan, as well as the Gui'an New Area (Figure 1).

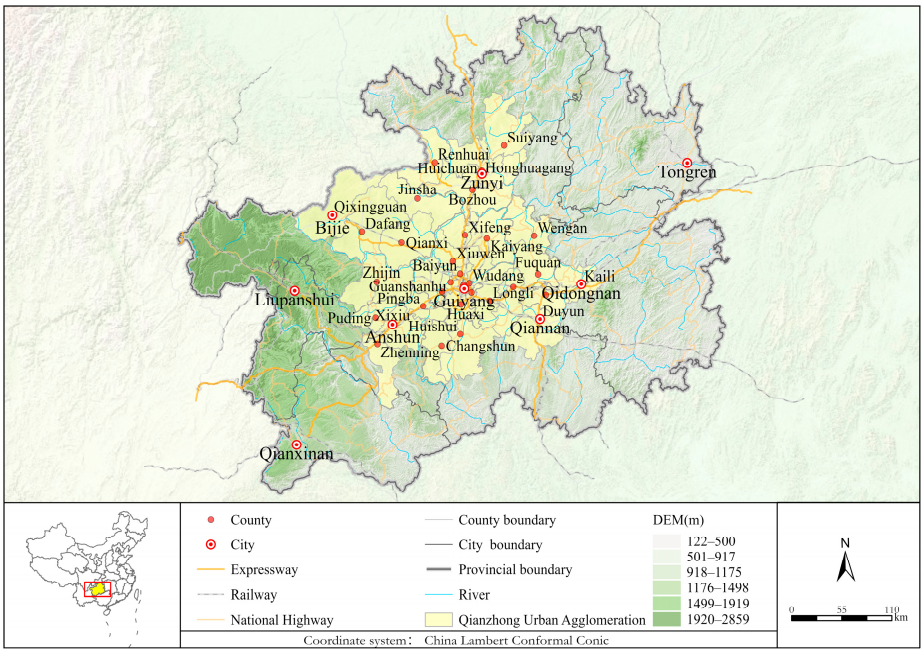


Figure 1. Location of the study area.

As a key demonstration region for China's new-type urbanization strategy, an important node of the Yangtze River Economic Belt, and a core area of the new round of Western Development, the Guizhou Central Urban Agglomeration also serves as a major spatial platform for Guizhou Province's national ecological civilization pilot zone, big data comprehensive experimental zone, and inland open economic pilot zone. It plays a significant role in driving sustained economic growth and promoting regional coordination within the province. As of 2024, the permanent resident population reached 18.85 million, with a regional gross domestic product (GDP) of 1.2134 trillion CNY, accounting for 48.5% and 60.2% of the provincial totals, respectively. The region represents the primary concentration area of population and economic activities in Guizhou Province. From 2000 to 2024, the urbanization rate increased from below 30% to over 60%, accompanied by a substantial expansion of construction land. Consequently, the area has become one of the most active regions of land use and land cover change (LUCC) within China's karst-dominated urban agglomerations. This rapid urbanization process has been strongly associated with the expansion of construction land driven by industrial development, infrastructure investment, and population agglomeration, which are key factors contributing to increased carbon emissions in the region. However, the region is predominantly mountainous, characterized by a high proportion of rugged terrain, limited land resources, and ecological fragility. These constraints pose significant challenges to urban development. Therefore, optimizing

land use patterns and achieving regional carbon balance are critical for promoting green and sustainable development in the Central Guizhou Urban Agglomeration.

2.2. Data Source and Processing

2.2.1. Land Use Data

The land use data used in this study were obtained from China's Land-Use/Cover Datasets (CLUD) (https://zenodo.org/records/18180184, accessed on 16 October 2025). The dataset was developed based on the Google Earth Engine cloud computing platform and derived from the interpretation of Landsat series imagery. It provides an overall classification accuracy exceeding 90% with a spatial resolution of 30 m × 30 m and adopts the WGS-1984 geographic coordinate system. The dataset effectively captures medium- to long-term land use and land cover changes across China. Six temporal snapshots of land use data (2000, 2005, 2010, 2015, 2020, and 2024) were selected for analysis. Using the vector boundary of the Central Guizhou Urban Agglomeration, the original land cover data were spatially clipped to the study area. To meet the objectives of this study, the original land cover categories were reclassified into six unified land use types: cultivated land, forest land, grassland, water bodies, construction land, and unused land. Finally, the coordinate system was transformed from WGS-1984 to the China Geodetic Coordinate System 2000 (CGCS2000).

2.2.2. POIs Data

Points of interest (POIs) are specific places or geographic entities marked on maps, typically including information such as name, category, and spatial coordinates, and they can effectively reflect the intensity and distribution of social and economic activities. POI data were retrieved from Gaode Map (https://www.amap.com/, accessed on 30 September 2025), which is the largest desktop and mobile map service provider in China. Using Gaode Map's application programming interface (API), we obtained a total of 3,468,327 POI records for two representative years, 2014 and 2024. Gaode Map classifies POIs into 23 categories based on their Chinese semantic phrases. All POI records were unified to the China Geodetic Coordinate System 2000 (CGCS2000).

2.3. Methods

2.3.1. Carbon Budget Calculation Principles

Carbon budget (*CB*) is defined as the difference between carbon emissions and carbon sequestration. Within a given territorial space, a $CB > 0$ indicates a net carbon source; whereas $CB < 0$ indicates a net carbon sink; and when $CB = 0$, it represents carbon balance. Changes in carbon budgets induced by land use/cover change (LUCC) can be characterized by comparing carbon coefficients (α_k) before (p_1) and after (p_2) land use transitions. According to the direction of carbon budget variation, four scenarios can be distinguished (Figure 2):

(1) When $\alpha_{p1} < \alpha_{p2}$ and the area is a carbon source (CB > 0), carbon emissions increase, forming a carbon-increment space.
(2) When $\alpha_{p1} > \alpha_{p2}$ and the area is a carbon source (CB > 0), carbon emissions decrease, representing a carbon-reduction space.
(3) When $\alpha_{p1} < \alpha_{p2}$ and the area is a carbon sink (CB < 0), carbon sequestration weakens (i.e., the system shifts toward higher net emissions), constituting a carbon-increment space.
(4) When $\alpha_{p1} > \alpha_{p2}$ and the area is a carbon sink (CB < 0), carbon sequestration is enhanced, leading to a carbon-reduction space.

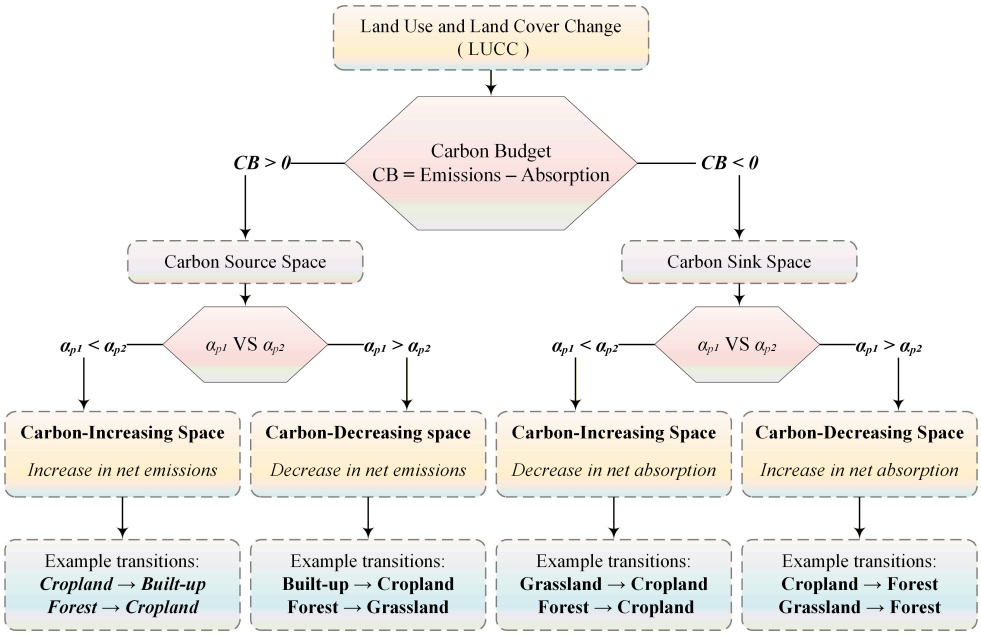


Figure 2. Relationship between LUCC and the carbon budget.

These scenarios indicate that carbon-increment and carbon-reduction effects may occur in both carbon source and carbon sink areas, reflecting the dynamic impacts of land use transitions rather than the intrinsic properties of land use types. Through appropriate adjustment of land use patterns, carbon budgets can be steered toward more favorable trajectories. The sustained expansion of carbon-reduction spaces constitutes a fundamental pathway toward achieving carbon neutrality.

Land use transition is the fundamental process underlying carbon budget differentiation within the same territorial space. Different land use categories exhibit distinct carbon emission and sequestration intensities, which are represented by their respective carbon coefficients (Table 1). At the grid scale, land use conversion during a given period alters the local carbon budget by changing net carbon emissions or sequestration. The magnitude of this change can be quantified as the difference between the carbon coefficients before and after conversion, which is defined in this study as the composite carbon coefficient. Based on the composite carbon coefficient, carbon budget variation can be calculated at the grid level and subsequently aggregated to characterize overall regional-scale changes. By integrating the remote sensing-based carbon density method with composite carbon coefficient correction, this approach enables spatially explicit carbon accounting at the grid level and supports the analysis of transition-related patterns of carbon budget variation under different land use configurations. Accordingly, the carbon budget is treated here as a territorial, land-use-based spatial accounting concept that captures the balance between carbon emissions and carbon sequestration under land use transitions, rather than as a full carbon-cycle or ecosystem process-based simulation.

Table 1. Carbon coefficients of different land use types [39–44].

Land Use Type	Carbon Coefficient (kg m^{-2} yr^{-1})	Description
Cultivated land (CRL)	0.0422	Agricultural land, including paddy fields and dry cropland
Forest land (FL)	−0.0578	Forests, including woodland, shrubland, and sparse forest
Grassland (GL)	−0.0021	Grass-dominated ecosystems

Table 1. *Cont.*

Land Use Type	Carbon Coefficient (kg m^{-2} yr^{-1})	Description
Water bodies (WA)	−0.0253	Natural water bodies and hydraulic facilities
Construction land (COL)	4.297	Urban residential, industrial, and transportation land
Unused land (UL)	−0.0005	Sandy land, saline-alkali land, bare land

2.3.2. Carbon Budget Accounting Method

To achieve fine-scale grid-level accounting of carbon budgets induced by land use/cover change (LUCC), the conventional remote sensing-based carbon density method is applied to all land use types to estimate net carbon emissions or sequestration. The calculation formula is expressed as follows [45]:

$$CB_i = \sum_{k,i=1}^{n} L_{ki} \times \alpha_{ki} \tag{1}$$

where CB_i represents the carbon budget of region i; L_{ki} denotes the area of land use type k within region i; and α_{ki} is the carbon coefficient corresponding to land use type k in region i, see Table 1.

Then, the conventional remote sensing-based carbon density method is refined using a composite carbon coefficient approach, and the calculation formula is expressed as follows:

$$CB_i = \sum_{i,j=1}^{m} S_{ij} \times \Delta\alpha_{ki} = \sum_{i,j=1}^{m} S_{ij} \times \left(\alpha_{p_2,j} - \alpha_{p_1,j}\right) \tag{2}$$

where m denotes the total number of land parcels in region i that experienced land use transitions; S_{ij} represents the area of parcel j in region i where land use change occurred; and $\alpha_{p_2,j} - \alpha_{p_1,j}$ is the composite carbon coefficient derived from the difference between the carbon coefficients at the final stage p_2 and the initial stage p_1 for parcel j.

2.3.3. Carbon Budget Index Classification Method

When accounting for carbon budget changes induced by land use and land cover change (LUCC), it is necessary to capture both the direction of change in carbon budgets resulting from land conversion (denoted as *DCCB*) and the rate of change in carbon budgets (denoted as *RCCB*) [41]. Based on this principle, a carbon budget index (*CBI*) was constructed to comprehensively evaluate carbon budget levels through classification of *CBI* values. The calculation formulation is expressed as follows:

$$\begin{cases} CBI = DCCB \times RCCB \\ DCCB = Sign\left(\alpha_{p2} - \alpha_{p1}\right) \\ RCCB = \left|\frac{\alpha'_{p1}}{\alpha'_{p2}}\right|, \left(\alpha'_{p1} > \alpha'_{p2}\right) \text{ or } \left|\frac{\alpha'_{p2}}{\alpha'_{p1}}\right|, \left(\alpha'_{p1} \le \alpha'_{p2}\right) \end{cases} \tag{3}$$

where *Sign* denotes the sign function. When $\alpha_{p1} < \alpha_{p2}$, $DCCB = 1$, indicating that the land use transition leads to an increase in carbon emissions (Carbon-increment space); when $\alpha_{p1} > \alpha_{p2}$, $DCCB = -1$, indicating that the land use transition results in enhanced carbon sequestration (Carbon-reduction space); when $\alpha_{p1} = \alpha_{p2}$, $DCCB = 0$, indicating no change in the carbon budget. The term α' represents the standardized form of α, obtained using the efficacy coefficient range normalization method.

Higher CBI values indicate greater LUCC-induced carbon emissions, whereas lower values reflect reduced emissions or enhanced carbon sequestration. CBI thus provides

a quantitative measure of carbon budget variations associated with LUCC. Using the equal-interval classification method, CBI values were categorized into three types: carbon-reduction space, no change space, and carbon-increment space, and further subdivided into nine levels (see Table 2).

Table 2. Classification thresholds for the carbon budget index (CBI).

Category	Weak (IV)	Moderate (III)	Strong (II)	Very Strong (I)
Carbon-Reduction Space	[−1.1, 0)	[−2.2,−1.1)	[−3.3,−2.2)	<−3.3
No Change		0		
Carbon-Increment Space	(0, 1.1]	(1.1, 2.2]	(2.2, 3.3]	>3.3

2.3.4. Identification of Key Monitoring Factors and Carbon Risk Analysis

Identification of Carbon Budget Driving Factors

During the study period, changes in construction land (including both conversion-in and conversion-out) accounted for 90.34% of the total variation in regional carbon budgets within the Central Guizhou Urban Agglomeration. Therefore, identifying the key drivers of carbon budget changes associated with construction land is essential for capturing the overall dynamics of regional carbon variations. Building upon the remote sensing-based carbon density accounting results, this study further identifies significant spatial entities that drive construction land expansion and examines how these driving factors affect carbon emissions across different types of construction land. In the empirical analysis, ordinary least squares (OLS) regression was first applied to explore the relationships between driving factors and the net carbon emissions induced by construction land expansion. Subsequently, quantile regression (QR) was employed to examine how these driving factors affect net carbon emissions at different conditional quantiles, thereby capturing heterogeneous effects across emission levels.

Point of interest (POI) data correspond directly to specific spatial entities within construction land and have been widely used in carbon emission accounting, built-up area monitoring, and land use mix analysis [46]. However, as POI data are point-based, they cannot directly reflect the actual land use scale of the corresponding geographic entities. Therefore, relying solely on POI counts to measure their spatial influence may lead to biased representations of different functional space types. To address this issue, and considering the regional characteristics and data availability in the Central Guizhou Urban Agglomeration, this study, with reference to previous studies [47], derived weights for different POI types based on the average land area proportion represented by each category. These weights were standardized to a 0–100 scale (Table 3), and the influence of each POI type was defined as the product of its quantity and corresponding weight. The influence of each POI type was defined as the product of its quantity and corresponding weight.

After data cleaning and preprocessing, the original POI dataset was categorized into 12 major types, including residential, catering, and shopping services. These 12 categories were further aggregated into six spatial units—residential, commercial-service, industrial, transportation, public service, and recreation (Table 3), which were used as driving factors of carbon budget variation. Based on this classification framework, regression models were constructed to quantify the relationship between POI influence and the net carbon emissions induced by construction land expansion. The calculation formula is as follows:

$$Q_{Y_{ij}}((\theta_k)|S_{it}) = \alpha_i + \sum_{j,i=1}^{n} \beta_{j\theta} S_{it} \times \varepsilon_i \quad (4)$$

where $Q_{Y_{i,t}}(\theta_k \mid S_{i,t})$ denotes the conditional quantile of the dependent variable $Y_{i,t}$ at the θ_k-th quantile; $S_{i,t}$ represents the vector of exogenous variables for parcel i in year t; and θ_k indicates the selected quantile level, with the 5th, 25th, 50th, 75th, and 95th percentiles adopted in this study. The term $\beta_{j,\theta}$ denotes the estimated coefficient vector at quantile θ; i indexes the spatial parcel; j represents the type of explanatory variable; and t denotes the study year. The parameter α_i captures unobserved individual (parcel-level) effects, while $\varepsilon_{i,t}$ is the error term.

Table 3. Correspondence between POI categories and construction land spatial types.

Level-1 Land Use Category	Land Use Characteristics	Level-2 Land Use Category	POI Category	POI Subcategory	Weight
Residential Space (LIS)	Low-, medium-, and high-rise residential areas, typically in contiguous distribution	Residential land	Commercial housing	Residential communities	50
Commercial-Service Space (CS)	Low-rise buildings are densely distributed with restaurants, clothing shops, and retail stores; high-rise buildings are mainly used for integrated office functions	Commercial facilities land	Catering services	Chinese and international restaurants	10
			Accommodation services	Hotels and guesthouses	10
			Shopping services	Shopping malls, supermarkets, building material markets, specialty commercial streets	15
		Business facilities land	Financial and insurance services	Banks, insurance, securities, and related institutions	30
			Science and cultural services	Media institutions	30
Industrial Space (IS)	Production workshops, warehouses, and supporting facilities of industrial and mining enterprises; a large land area with clear boundaries	Industrial land	Industrial Park	Industrial parks	70
			Company enterprises	Factories and enterprises	30
Transportation Space (TS)	Passenger and freight transport stations; distinct spatial form	Transportation facilities land	Transportation service facilities	Ports, airports, railway/bus stations, service areas	15
Public Service Space (PS)	Education, culture, healthcare, and administrative facilities, generally large land parcels	Administrative office land	Government and social organizations	Government agencies, foreign institutions, and social organizations	30
		Cultural facilities land	Science and cultural services	Museums, exhibition halls, libraries	30
		Educational and research land	Science and cultural services	Schools, research institutes, training institutions	30
		Medical and healthcare land	Healthcare services	Hospitals and disease prevention institutions	20
		Sports and leisure land	Sports and recreation services	Stadiums, resorts, cinemas, entertainment venues	10
Recreational Space (RS)	Parks, green spaces, plazas, scenic areas	Green space and plaza land	Scenic spots	Parks, scenic areas, plazas	95

Carbon Budget Monitoring and Early-Warning Index Construction

Constructing a composite index based on identified driving factors is a widely used approach for detecting variations in carbon emissions [12,48,49]. Based on the identified drivers of carbon budget, a carbon budget monitoring and Early-Warning Index (CB-MEWI) was established to evaluate carbon budget dynamics. The formulation is expressed as follows:

$$IT_Q = \sum_{i=1}^{n} W_{iQ} I_{iQ} \quad (5)$$

where IT_Q denotes the monitoring and early-warning index at quantile Q. A higher value of IT_Q indicates greater net carbon emissions induced by construction land expansion and, consequently, a higher carbon risk level. W_{iQ} represents the weight assigned to the i Level-1 spatial category at quantile Q, which is determined based on the estimated coefficients derived from the OLS and QR models. I_{iQ} denotes the standardized influence value of the i POI category at quantile Q.

Carbon Risk-Level Classification

Several approaches are commonly used to determine risk-level thresholds, including the comparison method, fluctuation method, parameter-based method, and error theory method [12,50]. The comparison and fluctuation methods typically rely on a single threshold to classify warning conditions, simply distinguishing between warning and non-warning states. The parameter-based method selects parameters that are highly correlated with the monitoring indicator and exhibit significant threshold characteristics to define warning levels. In contrast, the error theory method, grounded in the principles of normal distribution, classifies warning levels according to the degree of deviation of monitoring indicators from the mean value, with values exceeding one standard deviation commonly identified as anomalous.

In practical applications, the warning accuracy corresponding to each method is calculated separately to determine the optimal threshold classification approach. In this study, the accuracy of warning identification was evaluated by computing the overlap ratio between warning areas identified by the monitoring and early-warning index and the actual warning areas of construction land carbon emissions (Table 4).

Table 4. Risk-level classification threshold and accuracy assessment.

Methods	Classification Principle	Operational Procedure	Accuracy
Comparison Method	Median-based principle	Values greater than the median are classified as a warning.	57.77%
	Mean-based principle	Values greater than the mean are classified as a warning.	35.14%
Fluctuation Method	Range-based principle	$PW = min + (max - min) \times 0.75$ (6)	5.88%
Parameter-Based Method	Parameter-based classification	Carbon emissions from construction land were classified into five levels using the natural breaks (Jenks) method. The grid-based values of each level were used as thresholds to classify IT into five risk categories: no risk, low risk, moderate risk, high risk, and extremely high risk.	16.67%
Error Theory Method	Normal distribution-based principle	IT was classified into five risk categories (no, low, moderate, high, extremely high) based on deviations from the mean using different multiples of the standard deviation.	87.76%

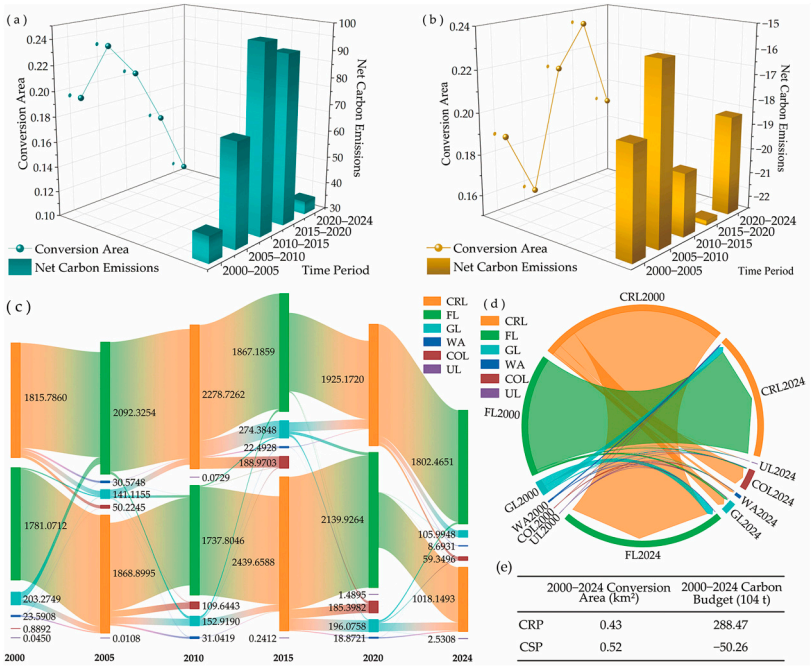
Note: *min* and *max* denote the minimum and maximum values of IT, respectively. For the comparison and fluctuation methods, accuracy refers to the identification accuracy of warning areas. For the parameter-based and error theory methods, accuracy refers to the identification accuracy of extremely high-risk areas.

3. Results

3.1. Land Use Change and Carbon Budget Variation

As shown in Figure 3, from 2000 to 2024, 17.68% of the territorial space in the Central Guizhou Urban Agglomeration experienced land use change, corresponding to an area of 0.95×10^4 km^2. Land use transitions were dominated by mutual conversions between cultivated land and forest land. Specifically, the conversion from cultivated land to forest land covered 0.46×10^4 km^2, accounting for 48.28% of the total changed area, while forest

land converted to cultivated land covered 0.34 × 10^4 km^2, representing 36.22%. In addition, the conversion from cultivated land to construction land covered 0.06 × 10^4 km^2 (5.90%), yet its carbon emission effect was significantly greater than that of other transition types. In terms of carbon effects, between 2000 and 2024, net carbon emissions in carbon-increment spaces increased by 2.8847 million t, whereas those in carbon-reduction spaces decreased by 0.5027 million t, resulting in an overall net increase of 2.3821 million t in the Central Guizhou Urban Agglomeration. Although conversions between cultivated land and forest land dominated in terms of area, transitions between cultivated land and construction land were the primary drivers of changes in net carbon emissions. The conversion from cultivated land to construction land contributed an increase of 2.3860 million t of net carbon emissions, accounting for 82.71% of the total increase in carbon-increment spaces. In contrast, the conversion from construction land to cultivated land reduced net carbon emissions by only 0.0020 million t, representing merely 0.39% of the total reduction in carbon-reduction spaces. The magnitude of increase was approximately 211 times greater than that of the reduction, indicating that under continued urbanization and large-scale conversion of cultivated land to construction land, substantially intensified carbon emission effects in carbon-increment spaces. The increase far exceeded the emission reduction achieved in carbon-reduction spaces, ultimately driving a continuous rise in overall net carbon emissions across the Central Guizhou Urban Agglomeration.



	2000–2024 Conversion Area (km^2)	2000–2024 Carbon Budget (104 t)
CRP	0.43	288.47
CSP	0.52	−50.26

Figure 3. Major land use transition areas and associated carbon budget changes in the Central Guizhou Urban Agglomeration. Note: Panels (**a**,**b**) show the major land use transition areas and corresponding carbon budget changes in carbon-increment spaces and carbon-reduction spaces for each time period, respectively. The units are 10^4 km^2 and 10^4 t. Panel (**c**) presents the transition areas of major land use types for each time period (unit: km^2). Panel (**d**) illustrates the chord diagram of major land use transitions over the entire study period. Panel (**e**) depicts the transition areas and corresponding net carbon emissions in carbon-increment spaces (CRP) and carbon-reduction spaces (CSP) over the entire study period.

As shown in Figure 4, land use change in the Central Guizhou Urban Agglomeration exhibited pronounced stage-wise dynamics over the study period. The area of land use change increased from 0.38 × 10^4 km^2 during 2000–2005 and peaked at 0.42 × 10^4 km^2 during 2010–2015, before declining to 0.30 × 10^4 km^2 during 2020–2024. Correspondingly, the

net increase in carbon emissions induced by land use change showed a "rise–fall" pattern, increasing from 0.2147 million t during 2000–2005 to 0.7822 million t during 2010–2015, and then decreasing markedly to 0.1621 million t during 2020–2024. From the perspective of functional spatial categories, net carbon emissions contributed by carbon-increment spaces rose continuously from 0.3963 million t during 2000–2005 to a peak of 0.9823 million t during 2010–2015, followed by a decline to 0.3476 million t during 2020–2024. This pattern was jointly driven by the net expansion of construction land and the net reduction in cultivated land. Specifically, the net increase in construction land expanded from 0.0050 $\times$ 10^4 km^2 during 2000–2005 to 0.0189 $\times$ 10^4 km^2 during 2010–2015, and subsequently decreased to 0.0059 $\times$ 10^4 km^2 during 2020–2024. Meanwhile, the net reduction in cultivated land increased from 0.1869 $\times$ 10^4 km^2 during 2000–2005 to 0.2149 $\times$ 10^4 km^2 during 2005–2010, before declining to 0.1018 $\times$ 10^4 km^2 during 2020–2024.

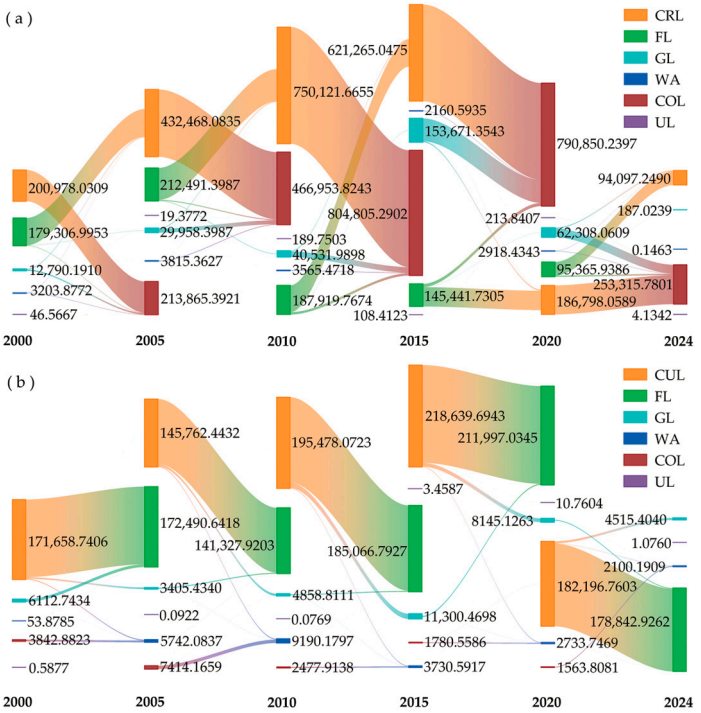


Figure 4. Net carbon emissions from major land use conversions in the Central Guizhou Urban Agglomeration. Panels (**a**,**b**) show the net carbon emissions of major land use types in carbon-increment spaces and carbon-reduction spaces, respectively, for each time period (unit: t). Transition area refers to the net area resulting from bidirectional conversions between two land use types. Net carbon emissions and net carbon sequestration were calculated using Equation (2). Only transition types or carbon budget changes with non-zero values are presented.

In contrast, the net reduction in carbon emissions associated with carbon-reduction spaces exhibited a pattern of gradual increase followed by a slight decline. The reduction increased from 0.1817 million t during 2000–2005 to 0.2230 million t during 2015–2020, before decreasing to 0.1855 million t during 2020–2024. This trend was primarily influenced by the combined effects of net increases in forest land and grassland, as well as net decreases in water bodies. Specifically, the net increase in forest land expanded from 0.1774 $\times$ 10^4 km^2 during 2000–2005 to 0.2140 $\times$ 10^4 km^2 during 2015–2020, and then slightly declined to 0.1802 $\times$ 10^4 km^2 during 2020–2024. The net increase in grassland rose from 0.0077 $\times$ 10^4 km^2 during 2000–2005 to 0.0255 $\times$ 10^4 km^2 during 2010–2015, before decreasing to 0.0102 $\times$ 10^4 km^2 during 2020–2024. Meanwhile, the net decrease in water bodies increased marginally from 0.0030 $\times$ 10^4 km^2 during 2000–2005 to 0.0031 $\times$ 10^4 km^2 during 2005–2010, and then declined to 0.0009 $\times$ 10^4 km^2 during 2020–2024 (Figure 4).

Overall, changes in forest land, grassland, and water bodies contributed to enhancing the emission-reduction effects of carbon-reduction spaces to some extent. However, their mitigating effects were insufficient to offset the substantial increase in net carbon emissions driven by the rapid expansion of construction land. As a result, the overall net carbon emissions in the Central Guizhou Urban Agglomeration continued to rise.

3.2. Spatial Characteristics of Carbon Budget Variation Under Different Land Use Transitions

3.2.1. CBI Classification and Corresponding Land Use Transition Directions

The carbon budget index (CBI) was calculated using Equation (3) and subsequently classified into hierarchical levels (Figure 5). Transitions between construction land and the other five land use types resulted in extremely strong carbon-increment or carbon-reduction spaces. Strong-level categories corresponded to conversions between forest land and cultivated land, grassland, or unused land. Weak-level categories were primarily associated with conversions between grassland and unused land. Moderate-level categories included all other land use transition types not encompassed by the above classifications.

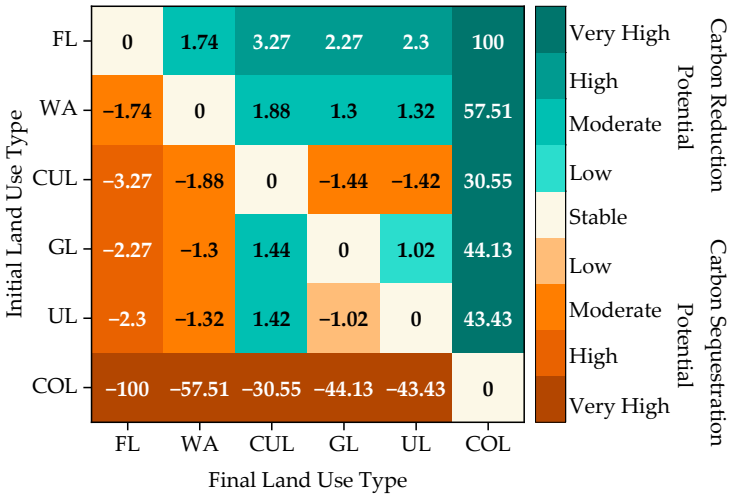


Figure 5. Comparison between CBI levels and land conversion type.

3.2.2. Carbon Budget Variation Characteristics Across Different CBI Levels

Based on the CBI classification results, land use transitions and associated net carbon emission changes during 2000–2024 were quantified (Table 5). Three major characteristics were identified. First, extremely strong-level parcels were the primary contributors to variations in net carbon emissions. The absolute values of the composite carbon coefficients for extremely strong parcels ranged from 4.25 to 4.36, far exceeding those of other parcel types. As a result, extremely strong carbon-reduction spaces accounted for only 0.06% of the total area during the study period and contributed merely 2.80% of the total net emission reduction. In contrast, extremely strong carbon-increment spaces accounted for 13.65% of the total area but contributed as much as 87.54% of the total increase in net carbon emissions. Furthermore, strong-level carbon-reduction spaces covered 93.08% of the total area and accounted for 93.77% of the total net emission reduction. These findings indicate that each unit increase (or decrease) in construction land would lead to an increase of 6.41 units (or a reduction of 44.34 units) in net carbon emissions. Second, except for extremely strong parcels, net carbon emissions associated with other parcel types generally remained stable or declined. During the study period, weak- and moderate-level parcels exhibited only marginal changes in net carbon emissions in both carbon-increment and carbon-reduction spaces. Strong-level parcels showed a net change of −0.1227 million t, which was negligible compared to the 2.5113 million t increase associated with extremely

strong parcels. This result underscores the dominant role of extremely strong parcels in regulating net carbon emissions. Third, the contribution of carbon-reduction spaces to the overall carbon balance exhibited a U-shaped trajectory over time. During 2000–2005, emission reductions in carbon-reduction spaces offset 45.84% of the emission increases in carbon-increment spaces. This proportion declined to 20.37% during 2010–2015 but rebounded to 53.35% during 2020–2024. The recovery can be attributed to the substantial increase in conversions from cultivated land to forest land, grassland, and water bodies, as well as from grassland to forest land, which significantly enhanced the emission-reduction effects of carbon-reduction spaces.

Table 5. Changes in area and net carbon emissions of different CBI classes in the Central Guizhou Urban Agglomeration.

CBI Category	CBI Level	Area (km^2)						Net Carbon Emission Change (10^4 t)					
		2000–2005	2005–2010	2010–2015	2015–2020	2020–2024	2000–2024	2000–2005	2005–2010	2010–2015	2015–2020	2020–2024	2000–2024
Carbon-Reduction Space	Very High	0.89	1.72	0.57	0.41	0.36	3.26	−0.38	−0.74	−0.25	−0.18	−0.16	−1.41
	High	1772.80	1429.43	1866.44	2139.52	1800.95	4809.79	−17.24	−14.13	−18.50	−21.20	−17.88	−47.13
	Moderate	107.78	139.63	277.67	201.01	111.79	354.14	−0.54	−0.67	−1.26	−0.92	−0.51	−1.73
	Low	0.01	0.00	0.02	0.08	0.23	0.01	0.00	0.00	0.00	0.00	0.00	0.00
No Change	Stable	49,963.51	49,917.11	49,611.01	49,852.26	50,790.98	44,278.78	0.00	0.00	0.00	0.00	0.00	0.00
Carbon-Increment Space	Low	0.00	0.02	0.16	1.24	2.50	0.18	0.00	0.00	0.00	0.00	0.00	0.00
	Moderate	112.74	99.67	109.19	155.86	146.11	228.95	0.53	0.45	0.49	0.70	0.68	1.07
	High	1780.22	2090.93	1734.13	1252.40	875.90	3520.15	17.72	20.73	17.26	12.48	8.75	34.86
	Very High	50.22	109.64	188.97	185.40	59.35	592.90	21.39	46.70	80.48	79.09	25.33	252.53

3.2.3. Spatiotemporal Evolution of CBI at the Grid Scale

As shown in Figure 6, the spatial distribution of CBI closely aligns with the pronounced core–periphery urbanization structure of the Central Guizhou Urban Agglomeration. Transitions between construction land and cultivated land primarily drove the formation of very high-level parcels. Very high carbon-increment spaces were mainly concentrated in the central city of Guiyang and Zunyi, whereas very high carbon-reduction spaces were predominantly distributed in non-built-up areas surrounding Guiyang, Zunyi, and Kaili. Across the five periods (2000–2005, 2005–2010, 2010–2015, 2015–2020, and 2020–2024), the conversion of cultivated land to construction land consistently dominated very high carbon-increment spaces, accounting for 94.05%, 92.70%, 93.30%, 78.76%, and 73.97% of the transition area, respectively. Correspondingly, this conversion contributed 93.97%, 92.61%, 93.21%, 78.56%, and 73.74% of total net emissions within very high carbon-increment spaces. Temporally, these spaces expanded progressively from core urban districts toward peripheral areas. In Guiyang, expansion occurred in a leapfrogging pattern toward Wudang, Huaxi, Qingzhen, Xiuwen, and Kaiyang, while in Zunyi it extended along the Honghuagang–Huichuan–Bozhou urban corridor.

Overall, very high carbon-increment spaces evolved from single-core concentration to multi-center expansion. Within very high carbon-reduction spaces, conversion from construction land to water bodies was overwhelmingly dominant, accounting for more than 96% of the transition area in each period and reaching 100% in 2020–2024. In contrast, conversion from construction land to cultivated land was negligible. Spatially, these reductions were concentrated in Guanshanhu, Yunyan, and Baiyun districts of Guiyang and in Honghuagang, Bozhou, Renhuai, and Suiyang of Zunyi. High-level parcels were primarily driven by mutual conversions between forest land and cultivated land, exhibiting strong spatial correspondence with the ecological "two barriers" (Wumeng–Miaoling and Dalou Mountain ecological barriers) and the "three river basins" corridors (Wujiang, Chishui River, and Qingshui River). High carbon-increment spaces were almost entirely composed of forest-to-cultivated land conversion (above 98% across all periods), accounting for more than 99% of net emissions within this category. These spaces were mainly distributed

in the Northwestern Wumeng–Miaoling barrier and the Southern Dalou Mountain barrier. Conversely, high carbon-reduction spaces were largely formed by cultivated-to-forest conversion, contributing over 96% of emission reductions in all periods and forming banded patterns along ecological barriers and river corridors. Moderate-level parcels were mainly associated with conversions between cultivated land and grassland. Moderate carbon-increment spaces were dominated by grassland-to-cultivated land conversion, accounting for more than 80% of transition areas in all periods and contributing the majority of associated net emissions.

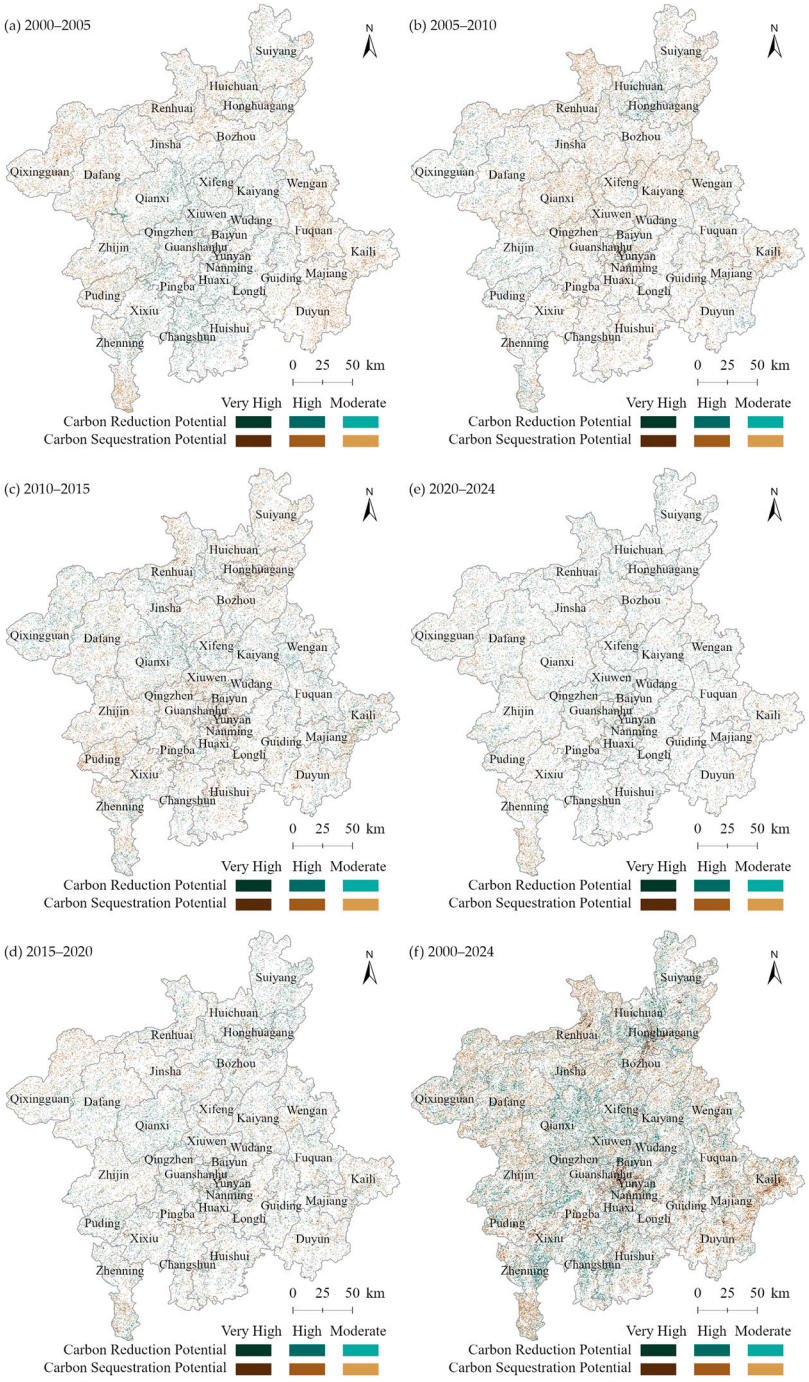


Figure 6. Spatial distribution of CBI in the Central Guizhou Urban Agglomeration. Note: Subfigures (**a**–**f**) depict the spatial distribution of CBI during 2000–2005, 2005–2010, 2010–2015, 2015–2020, 2020–2024, and 2000–2024 (the entire period), respectively.

Spatially, these areas were initially concentrated near the boundary between Qixingguan District and Dafang County, later shifting toward Jinsha County, Bozhou District, and Qianxi City. Moderate carbon-reduction spaces were mainly driven by cultivated-to-grassland and cultivated-to-water conversions. Cultivated-to-grassland conversion accounted for over 70% of transition areas and nearly 90% in later periods, contributing the majority of emission reductions. Cultivated-to-water conversion played a secondary role, particularly in earlier periods. These transitions were scattered across karst landform zones and ecological corridors, with relative concentration in the Qingshui River basin. Overall, the spatiotemporal evolution of CBI reflects the combined influence of urban expansion in core areas and ecological restoration in barrier and corridor regions, demonstrating strong functional differentiation between carbon source expansion and carbon sink enhancement.

3.3. Driving Factors and Risk Evaluation in Carbon-Increment Spaces

3.3.1. Identification of Driving Factors

Across the overall land use change process, very high carbon-increment spaces—defined as parcels converted from other land use types to construction land—accounted for 87.524% of the total net carbon emission increase within all carbon-increment spaces in the Central Guizhou Urban Agglomeration. This indicates that identifying the functional spatial characteristics associated with net emission growth induced by construction land expansion, and regulating such expansion accordingly, is critical for controlling overall net carbon emissions. In this study, newly added construction land within the study area was divided into 2187 grid cells of 3 km × 3 km. The net carbon emission increase in very high carbon-increment spaces was used as the dependent variable. The POI influence indices of six functional spatial categories—residential, commercial-service, industrial, transportation, public service, and recreational spaces—were initially considered as independent variables. Due to the temporal availability of POI data, the driver analysis was restricted to the period 2015–2024 to ensure temporal consistency between the explanatory variables and the modeled carbon emission changes. Ordinary least squares (OLS) and quantile regression (QR) models were constructed to examine the spatial associations between urban functional characteristics and net emission growth during 2015–2024. Multicollinearity diagnostics were performed prior to model estimation. The public service variable was excluded due to failing the variance inflation factor (VIF) test. The final model retained five explanatory variables: residential, commercial-service, industrial, transportation, and recreational spaces. All retained variables exhibited VIF values below the conventional threshold of 7.5, with an average value of 1.95, indicating acceptable collinearity levels and suitability for quantile regression analysis. Based on Equation (4), the relationships between independent variables and the dependent variable were further examined across different quantiles (Figure 7). The results show that as the quantile decreases, the spatial distribution of very high carbon-increment spaces transitions from a single-core, multi-polar pattern toward a more diffuse configuration with a gradual decline toward peripheral areas.

The OLS regression results (Table 6) indicate that all five urban functional spaces are significantly associated with net carbon emission increases, although their directions and magnitudes differ. Residential space exhibits the strongest positive association (coefficient = 0.814), suggesting that a one-unit increase in residential POI influence is associated with the greatest increase in grid-level net carbon emissions. Industrial space shows the second strongest positive association (coefficient = 0.648), indicating that the concentration of industrial functions tends to coincide with higher levels of carbon emission growth. Transportation space also demonstrates a significant positive association (coefficient = 0.242), indicating that the aggregation of transport infrastructure and mobility activities is generally associated with higher regional emission levels. Recreational space

has a positive but relatively small coefficient (0.072), implying a limited contribution to emission growth. In contrast, commercial-service space exhibits a significant negative association (coefficient = −0.388). This suggests that, within the Central Guizhou Urban Agglomeration, increases in commercial-service space do not coincide with increases in net carbon emissions from construction land and are instead associated with relatively lower emission growth. This pattern resembles that observed in rapidly industrializing and urbanizing regions, where development-oriented spaces dominated by residential and industrial expansion contribute most to emission growth, followed by transportation infrastructure. By comparison, commercial-service expansion tends to occur within existing built-up areas through infill development and urban renewal. As these areas transition toward more mature urban living environments, land development intensity stabilizes, and land use-induced carbon budget fluctuations become less pronounced. The observed spatial redistribution of very high carbon-increment spaces from central districts toward newly developed urban areas further supports this interpretation and is consistent with the statistically negative association between commercial-service space and net carbon emission growth.

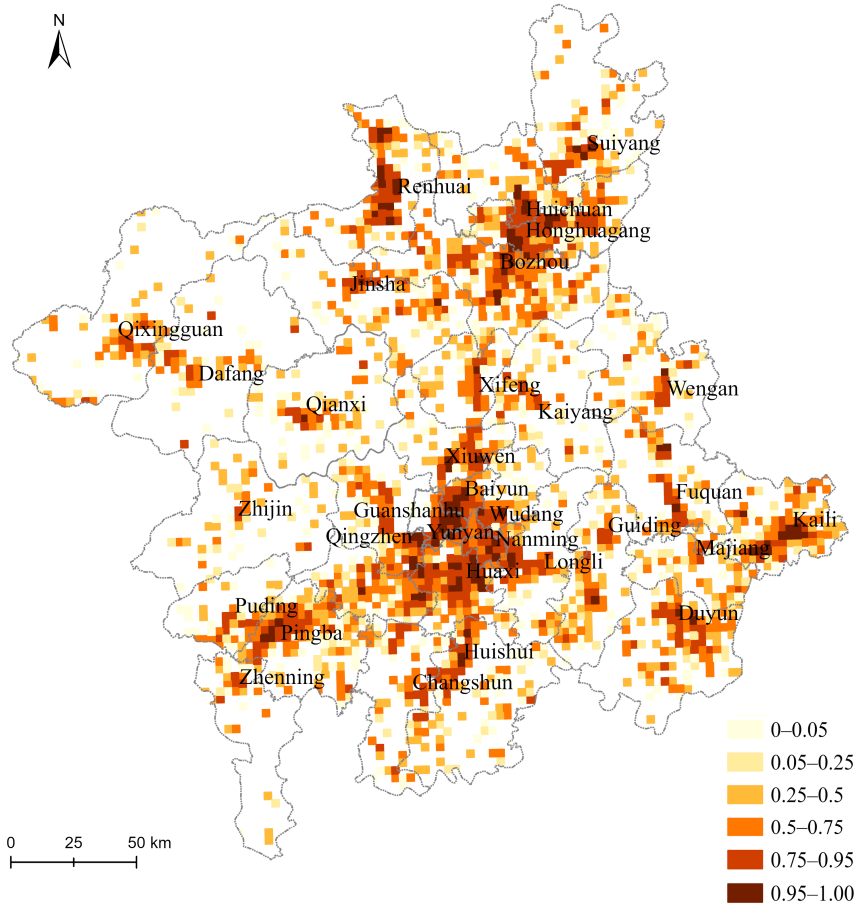


Figure 7. Grid-level distribution of very high carbon-increment spaces across different quantiles during 2015–2024.

The quantile regression (QR) results (Table 6) reveal clear heterogeneity across emission levels. The coefficients of residential, industrial, and transportation spaces increase significantly with rising quantiles, whereas the coefficient of recreational space becomes insignificant at higher quantiles. In contrast, the negative association of commercial-service space strengthens markedly as the quantile increases. At lower quantiles, where net carbon emission increases are relatively modest, the positive effect of residential space is compar-

atively weak. However, the effect intensifies progressively toward higher quantiles and reaches its maximum at the 0.95 quantile. This pattern indicates that under high carbon-increment conditions, residential functional intensity—together with associated building energy consumption, daily mobility demand, and supporting infrastructure—becomes more strongly associated with emission growth in high-emission grids. Industrial space shows a progressively stronger association across quantiles, especially in the upper quartiles. This suggests that high carbon-increment grids are closely associated with industrial agglomeration, supply chain clustering, and heavy industrial characteristics. Compared with OLS, the QR results more clearly reveal the stronger upper-tail association of industrial space with net carbon emission growth. The positive association of transportation space increases steadily with quantiles, reflecting that as regions enter stages characterized by intensive development, high commuting demand, and frequent logistics turnover, transport infrastructure density and mobility intensity become more strongly associated with emission growth in the upper tail. Recreational space shows relatively small coefficients overall and becomes statistically insignificant at the 0.95 quantile. This indicates that its influence is primarily concentrated in low- to mid-quantile grids. In earlier or lower-density contexts, recreational facilities—including green spaces and plazas—may contribute to localized carbon sequestration and microclimate improvement. However, at higher quantiles, the marginal mitigation effect of recreational space is insufficient to offset the spillover impacts of surrounding high-intensity land uses, resulting in diminished statistical significance. The negative effect of commercial-service space becomes increasingly pronounced in the mid-to-high quantiles, with a notably steeper slope after the 0.50 quantile. This suggests that service-oriented redevelopment, functional mixing, and improved energy-use efficiency associated with commercial-service expansion may reduce the marginal increase in net carbon emissions.

Table 6. OLS and QR results.

Driving Factors	OLS	QR				
		5th	25th	50th	75th	95th
Δ*LIS*	0.814 ***	0.108 ***	0.328 ***	0.770 ***	0.985 ***	1.259 ***
Δ*CS*	−0.388 ***	−0.124 ***	−0.122 ***	−0.442 ***	−0.700 ***	−1.129 ***
Δ*IS*	0.648 ***	0.155 ***	0.455 ***	0.940 ***	1.646 ***	2.975 ***
Δ*TS*	0.242 ***	0.083 ***	0.097 ***	0.324 ***	0.767 ***	1.158 ***
Δ*LES*	0.072 *	0.010 ***	0.030 ***	0.074 ***	0.050 *	0.123
Obs.	2187	2187	2187	2187	2187	2187

Note: ***, and * indicate significance at the 1%, 5%, and 10% levels, respectively.

3.3.2. Carbon Budget Early-Warning Evaluation

Based on the identified driving factors, this study conducted risk classification and grading of net carbon emission increases induced by construction land expansion to enhance the precision of risk management. Thresholds for warning levels were determined using the comparison method, fluctuation method, parameter-based method, and error theory method, respectively. Among these approaches, the error theory method achieved the highest warning identification accuracy (87.76%; Table 4). Accordingly, the warning thresholds of the monitoring index were subsequently determined using the error theory method (Table 7), and spatial identification of net carbon emission increase risk areas was performed (Figure 6). The spatial distribution of risk grids exhibits significant clustering patterns across different risk levels (Figure 8a). To further characterize spatial continuity, a kernel density clustering approach was applied to aggregate discrete risk grids into continuous risk zones (Figure 8b). The results indicate that, across quantile intervals, high- and very high-risk areas are not only more likely to transition to higher-risk levels but also

represent the priority areas for focused monitoring and regulation within each interval (Figure 8c,d).

Table 7. Threshold classification of the carbon budget monitoring and early-warning index.

Risk Threshold Interval	No Risk	Low Risk	Moderate Risk	High Risk	Very High Risk
	$(-\infty, \mu - \sigma)$	$[\mu - \sigma, \mu - 0.5\sigma)$	$[\mu - 0.5\sigma, \mu + 0.5\sigma)$	$[\mu + 0.5\sigma, \mu + \sigma)$	$[\mu + \sigma, +\infty)$
IT	(−∞, 0.6575)	[0.6575, 0.6710)	[0.6710, 0.6979)	[0.6979, 0.7114)	[0.7114, +∞)
ITQ, Q = 0.05	(−∞, 0.5442)	[0.5442, 0.5899)	[0.5899, 0.6813)	[0.6813, 0.7270)	[0.7270, +∞)
ITQ, Q = 0.25	(−∞, 0.6767)	[0.6767, 0.6783)	[0.6783, 0.6816)	[0.6816, 0.6832)	[0.6832, +∞)
ITQ, Q = 0.5	(−∞, 6835)	[0.6835, 0.6836)	[0.6836, 0.6839)	[0.6839, 0.6840)	[0.6840, +∞)
ITQ, Q = 0.75	(−∞, 0.6843)	[0.6843, 0.6846	[0.6846, 0.6851)	[0.6851, 0.6853	[0.6853, +∞)
ITQ, Q = 0.95	(−∞, 0.6863)	[0.2964, 0.6884)	[0.3275, 0.6926)	[0.6926, 0.6948)	[0.6948, +∞)

Note: μ and σ represent the mean and standard deviation, respectively.

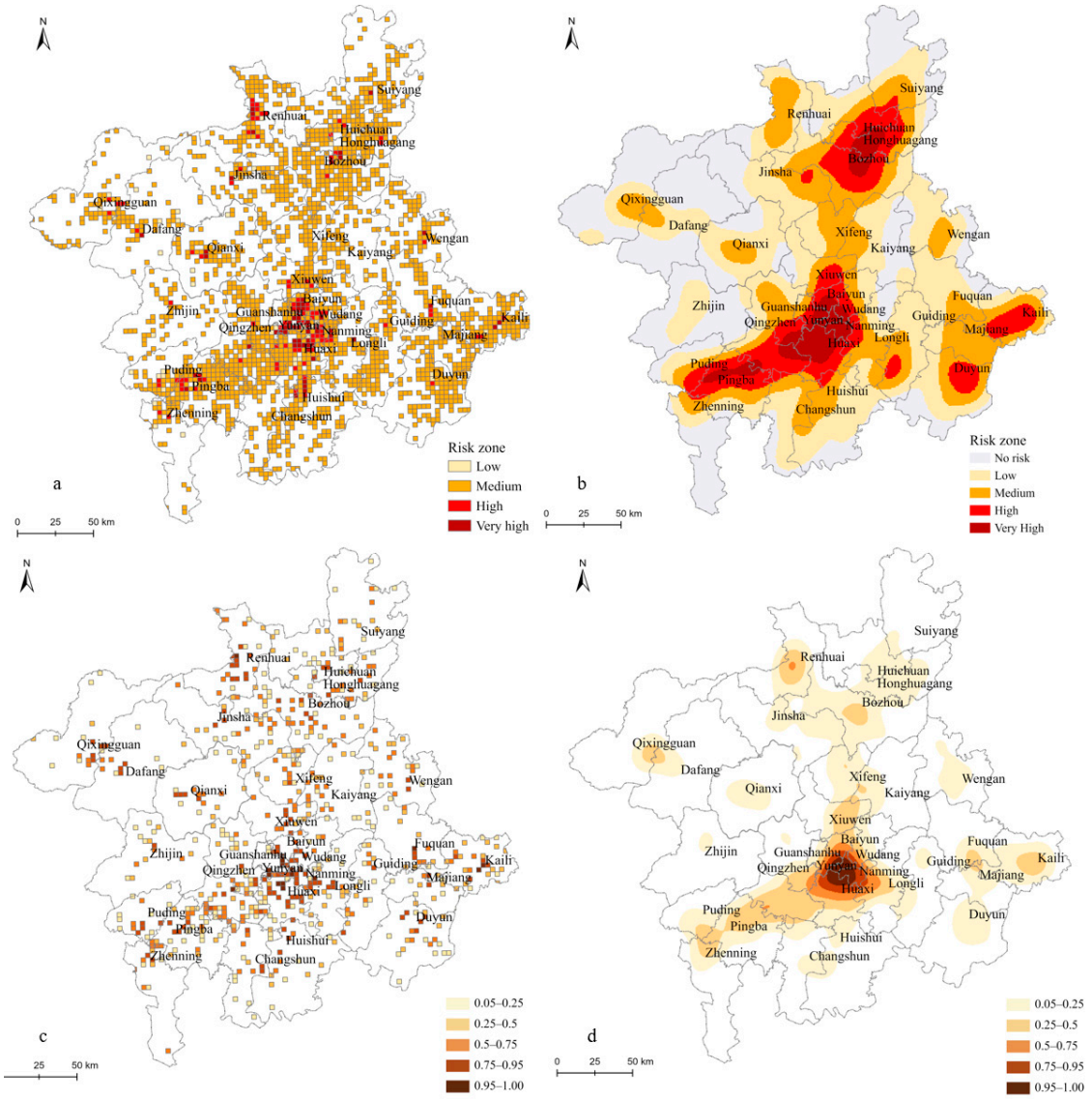


Figure 8. Risk zoning of net carbon emission increases from construction land expansion. Note: (**a**) Spatial distribution of risk grids at different risk levels; (**b**) risk zoning based on different risk levels; (**c**) spatial distribution of high- and very high-risk grids across different quantile intervals; (**d**) risk zoning of high- and very high-risk areas across different quantile intervals. Areas without color indicate no risk.

Risk levels and quantile intervals exhibit a pronounced core–periphery spatial pattern, decreasing from the urban cores of Guiyang, Zunyi, and Anshun toward the peripheral ecological zones characterized by the "two barriers" and "three river basins." This spatial gradient suggests differentiated governance priorities across regions and quantile intervals.

(1) Very high-risk areas are primarily concentrated in the central districts of Guiyang, Zunyi, and Anshun. These areas represent the most economically intensive and highly developed urban cores of the Guizhou Central Urban Agglomeration, where land development remains active, and energy consumption and transport-related emissions are concentrated. Spatial optimization in these areas should prioritize compact development, functional integration, and intensified land use to enhance efficiency. Urban renewal, industrial restructuring, restrictions on energy-intensive projects, and promotion of green building standards and low-carbon mobility are critical for shifting core districts from high-energy growth toward quality-oriented, low-carbon transformation.

(2) High-risk areas form a ring-like distribution surrounding very high-risk cores and extend into peripheral growth zones, including parts of Duyun, Longli, Huishui, Kaili, Majiang, and Jinsha. These regions often serve as receiving areas for industrial relocation and population redistribution, functioning as expansion frontiers of the urban agglomeration. Preventing carbon leakage associated with industrial transfer is essential. Measures should include stricter entry standards for high-emission industries, low-carbon upgrading of industrial parks, and promotion of green manufacturing and circular economy practices. In peripheral areas, controlling low-density sprawl and maintaining ecological buffer zones are important for preserving landscape connectivity.

(3) Moderate-risk areas are widely distributed along the outer margins of high-risk zones, including Renhuai, Qixingguan, Dafang, Qianxi, and Wengan. These areas are typically located within urban–rural transition zones, characterized by moderate levels of industrialization and urbanization, relatively intact ecological backgrounds, and increasing development pressure. Strengthening ecological redline protection, land use regulation, and preservation of permanent basic farmland and wetlands is essential. Promoting eco-agriculture, forestry-based carbon sequestration, and low-carbon rural development can enhance the balance between emission growth and ecological carrying capacity.

(4) Low-risk areas are mainly located in mountainous and hilly regions at the outer edges of the urban agglomeration, where urbanization intensity is relatively low, and ecosystems remain largely intact. These areas function as important carbon balance buffers. Strict control over the conversion of ecological land (forest, grassland, and water bodies) and reinforcement of protected-area systems are necessary to prevent disorderly expansion. Developing eco-agriculture, under-forest economies, and rural tourism can enhance ecological value while maintaining sustainable economic returns.

(5) No-risk areas are predominantly distributed in outer ecological function zones, such as forest reserves, water conservation areas, and high-altitude mountainous regions, which play a crucial role in regional ecological security. Establishing baseline ecological databases, enforcing ecological protection boundaries, and strengthening dynamic ecosystem monitoring are essential to prevent ecological degradation.

(6) At quantiles above the 0.50 level, higher-risk grids are particularly concentrated in Yunyan, Guanshanhu, Nanming, and Huaxi districts of Guiyang. Compared with the overall risk pattern, high- and very high-risk areas exhibit stronger spatial clustering in these districts. These areas are therefore likely to represent focal zones for controlling future net carbon emission growth. Establishing high-density monitoring networks and strengthening sector-specific emission regulations can facilitate differentiated

and hierarchical carbon governance led by core urban centers and coordinated with peripheral regions.

4. Discussion

This study developed a grid-based fine-scale carbon budget accounting model for the Central Guizhou Urban Agglomeration using a composite carbon coefficient approach and systematically examined the mechanisms through which land use change drives regional net carbon emissions. The results indicate that construction land expansion is the dominant factor contributing to the carbon budget imbalance. In particular, the conversion of cultivated land to construction land accounted for 87.54% of the net carbon emission increase in extremely strong carbon-increment spaces. This finding is consistent with previous studies in the Yangtze River Delta and Chengdu–Chongqing urban agglomerations, further confirming that construction land growth is the principal driver of carbon source expansion in urban agglomerations [12,44,51]. From the perspective of territorial spatial planning, these findings suggest that limiting disorderly construction land expansion, particularly the conversion of cultivated land into built-up areas, is critical for mitigating regional carbon budget imbalance.

However, unlike plain-type urban agglomerations, the Central Guizhou Urban Agglomeration, characterized by a typical karst mountainous landscape, exhibits a distinctive spatial configuration in which a core–periphery urban structure is intertwined with the ecological pattern of the "two barriers and three river basins." This reflects strong regional specificity in carbon budget distribution. Traditional carbon accounting methods often struggle to capture fine-scale carbon dynamics in fragmented mountainous landscapes [32]. By integrating 30 m × 30 m land use data with POI-derived spatial functional weights, this study achieves grid-level representation of carbon budgets and improves the characterization of spatial heterogeneity. These findings highlight the importance of high-resolution spatial data in regional carbon budget assessment [12,33]. More importantly, they indicate that spatial planning in mountainous urban agglomerations should not simply replicate the expansion-oriented planning logic commonly observed in plain-based urban systems. Instead, planning strategies need to account for the fragmented, corridor-like, and ecologically constrained nature of land development in mountainous terrain. In this context, high-risk carbon-increment spaces identified in this study can provide a spatial basis for delineating key control zones, optimizing development boundaries, and strengthening ecological protection in areas vulnerable to construction land encroachment.

Quantile regression results further demonstrate that industrial and transportation spaces are more strongly associated with carbon emissions associated with construction land expansion, with regression coefficients increasing toward higher quantiles. This suggests that high-emission areas are more sensitive to functional land use changes, consistent with previous findings on the carbon amplification effects of industrial agglomeration in Southwestern China. Methodologically, this study establishes an integrated analytical framework linking carbon budget indices, spatial association analysis, and monitoring early-warning mechanisms. The composite carbon coefficient approach enables dynamic grid-level simulation while refining generalized land use categories into functional spatial units through POI weighting. Compared with nighttime light data, which often fail to distinguish land use functions [52,53], this approach enhances the spatial interpretability of land use-related carbon budget variation. Although similar strategies have been applied in the Chengdu–Chongqing urban agglomeration [12], systematic integration of multi-quantile regression at the grid scale remains limited. The results further reveal amplified emission effects of residential and industrial spaces at higher quantiles, deepening the understanding of spatial heterogeneity in urban core carbon source intensity. In addition, the

error theory-based threshold method achieved an identification accuracy of 87.76%, outperforming parameter-based and fluctuation approaches, suggesting the strong applicability of normal distribution-based classification in regional carbon risk monitoring.

Despite these advances, several limitations remain. First, carbon coefficients were derived primarily from established literature and provide a reasonable basis for regional-scale carbon budget accounting; however, further localization may improve the representation of soil carbon pool characteristics and vegetation carbon density heterogeneity in karst regions. Future studies should incorporate field observations and remote sensing inversion methods, drawing on global carbon inventory techniques [54], to refine region-specific carbon density parameters. Second, although POI data can effectively represent the functional structure of urban space, relying solely on POI indicators may not fully capture the complexity of urban functional activities. Future studies should integrate multi-source spatiotemporal data, such as remote sensing imagery, population mobility data, and energy consumption data, to improve the representation of urban functions and the characterization of carbon emission processes [14]. Finally, while the monitoring and early-warning system effectively identifies high carbon risk areas, its integration with territorial spatial planning instruments requires further exploration [1], particularly in relation to ecological compensation and carbon trading mechanisms. Future studies should further strengthen the translation of grid-based carbon budget results into operational planning tools, such as ecological restoration prioritization, differentiated land use regulation, urban growth boundary adjustment, and low-carbon territorial spatial governance.

5. Conclusions and Policy Implications

5.1. Conclusions

This study improved the conventional remote sensing-based carbon density approach by introducing a composite carbon coefficient method, enabling fine-scale grid-level carbon budget accounting, and providing a clearer understanding of spatial patterns and relationships through which land use change is associated with net carbon emissions. Based on 30 m $\times$ 30 m land use data for the Central Guizhou Urban Agglomeration from 2000 to 2024, the spatiotemporal evolution of net carbon emissions associated with land use change was systematically examined. Key driving factors of construction land expansion were identified, and a carbon budget monitoring and risk early-warning framework was established. The main conclusions are as follows:

(1) Rational adjustment of land use structure is important for shaping territorial carbon functions. Effective regulation depends not solely on expanding carbon sink areas or reducing carbon source areas independently, but rather on enlarging carbon-reduction spaces while constraining the expansion of carbon-increment spaces.

(2) From 2000 to 2024, land use change in the Central Guizhou Urban Agglomeration resulted in a net carbon emission increase of 2.3821 million t, primarily associated with the conversion of cultivated land to construction land. Accelerated construction land expansion in the later stages significantly amplified net emission growth. Meanwhile, increases in ecological land, including forest and grassland, enhanced carbon-reduction spaces. The offsetting effect of carbon-reduction spaces relative to carbon-increment spaces exhibited a U-shaped trajectory over time, indicating a gradually strengthening contribution of carbon-reduction spaces to regional carbon balance.

(3) The spatial distribution of carbon-increment and carbon-reduction spaces closely corresponds to the core–periphery urbanization structure and the ecological configuration of the "two barriers and three river basins." Carbon-increment spaces are highly concentrated in the core urban areas of Guiyang and Zunyi, whereas carbon-reduction spaces are mainly distributed in surrounding rural and ecological barrier zones.

(4) Construction land expansion is strongly associated with net carbon emission growth. Industrial and transportation spaces significantly promote emission increases associated with construction land, while residential spaces also exhibit a strong positive relationship. In contrast, commercial-service space shows a negative association with net emission growth, reflecting its role as a relatively mature urban functional space with lower marginal carbon impacts.

(5) Based on the dominant associated factors, a carbon budget monitoring framework integrating risk identification, monitoring, evaluation, and risk management was developed. Key monitoring areas were identified in the core districts of Guiyang, Zunyi, and Gui'an New Area. The early-warning system achieved an identification accuracy of 87.76%, indicating good applicability in supporting fine-scale carbon management in mountainous urban agglomerations.

5.2. Policy Implications

Rapid urbanization in the Central Guizhou Urban Agglomeration has been associated with substantial changes in the spatial configuration of carbon sources and carbon sinks. The spatiotemporal differentiation of carbon budgets has become increasingly complex, posing higher demands for fine-scale accounting and precise regulation. To support regional carbon mitigation decision-making and territorial spatial governance, the following policy implications are proposed based on the findings of this study.

(1) Strengthening and institutionalizing the carbon budget monitoring framework. The composite carbon coefficient method enables grid-level carbon budget accounting and, through the integration of POI data, helps distinguish carbon budget variation across different functional types of construction land. This approach improves the spatial representation of land use-related carbon budget variation compared with conventional methods. It is therefore recommended that this framework be incorporated into the dynamic monitoring, evaluation, and early-warning system of territorial spatial planning, and gradually integrated into the "One Map" supervision platform for territorial spatial planning implementation. This integration would provide a useful planning reference for supporting real-time carbon monitoring and spatial decision-making. By integrating big data analytics and artificial intelligence techniques into comprehensive monitoring platforms, model parameters and algorithms can be iteratively optimized to enhance scenario simulation and predictive capabilities. Furthermore, continuous feedback calibration mechanisms should be developed to improve system robustness and support its application within China's "dual carbon" policy framework and territorial spatial governance system.

(2) Promoting low-carbon transformation of construction land development patterns. Given the pronounced core–periphery urban structure of the Central Guizhou Urban Agglomeration, differentiated strategies should be adopted to promote compact and multifunctional urban development. Enhancing vertical land use, improving green space integration, and increasing land use efficiency can mitigate the adverse carbon impacts of disorderly expansion. At the planning level, industrial land should transition toward intensive and clustered layouts to reduce emission pressures associated with spatial sprawl. In practice, these strategies may be implemented through urban renewal policies, redevelopment of inefficient land, and optimization of industrial park layouts within territorial spatial master planning. In extremely high- and high-risk carbon zones, mixed land use models may be encouraged to shorten commuting distances and reduce transport-related emissions, which may contribute to lower carbon pressures. Such approaches are consistent with existing planning tools aimed at promoting compact urban form and reducing transport-related carbon emissions.

(3) Coordinating cultivated land protection and ecological restoration.

In medium- to high-carbon-risk areas, strict control over the conversion of cultivated land to construction land is essential. Priority should be given to brownfield redevelopment, urban fringe land consolidation, and rural spatial restructuring, complemented by ecological compensation mechanisms that strengthen incentives for farmland protection. In medium- to low-risk areas, systematic restoration of ecologically fragile zones and key ecological corridors should be reinforced. These actions can be coordinated with ecological protection red lines and national ecological restoration programs to enhance implementation feasibility. The development of eco-agriculture, ecological tourism, and other green industries can enhance regional carbon sink capacity, improve ecosystem stability, and promote synergies between ecological conservation and economic development.

(4) Advancing cross-regional collaborative carbon governance.

Building upon fine-scale carbon budget accounting results, a cross-regional governance framework should be established that considers differentiated emission responsibilities, capacities, and mitigation potentials among cities. Clear allocation of roles and responsibilities in carbon reduction is essential. Through resource sharing, technological cooperation, and information exchange, a scientifically grounded carbon compensation mechanism may be developed to address carbon emission challenges in densely urbanized and peri-urban zones. This may be further supported by inter-city coordination mechanisms and regional policy frameworks for joint carbon reduction. Such collaborative governance can enhance overall emission-reduction efficiency and support coordinated low-carbon transition and high-quality development across the Guizhou Central Urban Agglomeration.

Author Contributions: Conceptualization, D.L., J.C. and Z.W.; methodology, software, formal analysis, validation, visualization, writing—original draft preparation, and visualization, D.L., J.C. and Z.W.; supervision and project administration, D.L. and Z.W.; investigation and data curation, D.L., J.C. and Z.S.; writing—review and editing, D.L., J.C. and F.W.; funding acquisition, D.L. All authors have read and agreed to the published version of the manuscript.

Funding: This research was funded by the Guizhou Provincial Basic Research Program (Natural Science), grant number ZK[2023]-461; the Doctoral Talent Fund Project of Tongren University, grant number tyxyDH2218; the Engineering Research Center of Intelligent Monitoring and Policy Simulation of Mountainous Land Space, Higher Education Institutions of Guizhou province, grant number 2023045; High level Innovative Talent Training Project of Guizhou Province (No. 2024-(2023)-076).

Data Availability Statement: The data presented in this study are available upon request from the corresponding author.

Conflicts of Interest: The authors declare no conflicts of interest.

References

1. Córdoba Hernández, R.; Camerin, F. The application of ecosystem assessments in land use planning: A case study for supporting decisions toward ecosystem protection. *Futures* **2024**, *161*, 103399. [CrossRef]
2. Seto, K.C.; Güneralp, B.; Hutyra, L.R. Global forecasts of urban expansion to 2030 and direct impacts on biodiversity and carbon pools. *Proc. Natl. Acad. Sci. USA* **2012**, *109*, 16083–16088. [CrossRef] [PubMed]
3. Wang, S.; Li, G.; Fang, C. Urbanization, economic growth, energy consumption, and CO_2 emissions: Empirical evidence from countries with different income levels. *Renew. Sustain. Energy Rev.* **2018**, *81*, 2144–2159. [CrossRef]
4. Yang, B.; Ma, X.; Li, J.; Yu, H.; Sui, H.; Chen, F.; Tan, L. The relationship between high-quality development and ecosystem health in China's urban agglomerations. *J. Environ. Manag.* **2025**, *377*, 124720. [CrossRef] [PubMed]
5. Grimm, N.B.; Faeth, S.H.; Golubiewski, N.E.; Redman, C.L.; Wu, J.; Bai, X.; Briggs, J.M. Global change and the ecology of cities. *Science* **2008**, *319*, 756–760. [CrossRef]
6. Lu, X.; Zhang, Y.; Li, J.; Duan, K. Measuring the urban land use efficiency of three urban agglomerations in China under carbon emissions. *Environ. Sci. Pollut. Res. Int.* **2022**, *29*, 36443–36474. [CrossRef]

7. Li, R.; Zhang, J.; Qu, X.; Liu, X. Spatiotemporal dynamics of land-use carbon emission efficiency in the Yangtze River Delta Urban Agglomeration: Insights from a directed weighted network. *J. Environ. Manag.* **2026**, *400*, 128719. [CrossRef]
8. Feng, X.; Wang, S.; Li, Y.; Yang, J.; Wu, X.; Zhang, Q.; Wang, X. Which urban expansion pattern dominates the variation of carbon emission performance?—Evidence from 244 cities in China. *J. Clean. Prod.* **2025**, *519*, 145984. [CrossRef]
9. Xu, H.; Li, X. Effect mechanism of Chinese-style decentralization on regional carbon emissions and policy improvement: Evidence from China's 12 urban agglomerations. *Environ. Dev. Sustain.* **2022**, *25*, 474–505. [CrossRef]
10. Zhu, Y.; Xia, X.; Canadell, J.G.; Piao, S.; Lu, X.; Mishra, U.; Wang, X.; Yuan, W.; Qin, Z. China's carbon sinks from land-use change underestimated. *Nat. Clim. Change* **2025**, *15*, 428–435. [CrossRef]
11. Li, J.; Huang, Y.; Liang, H.; He, L.; Du, H.; Zhu, J.; Zheng, B.; Wan, W. Refined assessment of carbon emissions from land use in China: A research framework based on "provincial accounting-efficiency assessment-spatial synergy". *Sustain. Cities Soc.* **2025**, *132*, 106831. [CrossRef]
12. Wei, Z.; Tu, J.; Xiao, L.; Yang, Y.; Li, Y. Detailed accounting of territorial carbon budgets and monitoring of driving factors in the Chengdu-Chongqing Urban Agglomeration. *J. Nat. Resour.* **2025**, *40*, 1294. [CrossRef]
13. Luo, H.; Gao, X.; Liu, Z.; Liu, W.; Li, Y.; Meng, X.; Yang, X.; Yan, J.; Sun, L. Real-time Characterization Model of Carbon Emissions Based on Land-use Status: A Case Study of Xi'an City, China. *J. Clean. Prod.* **2024**, *434*, 140069. [CrossRef]
14. Cao, R.; Huang, G.H.; Chen, J.P.; Li, Y.P. A fractional multi-stage simulation-optimization energy model for carbon emission management of urban agglomeration. *Sci. Total Environ.* **2021**, *774*, 144963. [CrossRef]
15. Ding, M.; Yang, X.; Zhao, R.; Zhang, Z.; Xiao, L.; Xie, Z. Optimization of territorial space pattern under the goal of carbon neutrality: Theoretical framework and practical strategy. *J. Nat. Resour.* **2022**, *37*, 1137. [CrossRef]
16. Gao, J.; O'Neill, B.C. Mapping global urban land for the 21st century with data-driven simulations and Shared Socioeconomic Pathways. *Nat. Commun.* **2020**, *11*, 2302. [CrossRef]
17. Hong, C.; Burney, J.A.; Pongratz, J.; Nabel, J.E.M.S.; Mueller, N.D.; Jackson, R.B.; Davis, S.J. Global and regional drivers of land-use emissions in 1961–2017. *Nature* **2021**, *589*, 554–561. [CrossRef]
18. Yue, C.; Ciais, P.; Houghton, R.A.; Nassikas, A.A. Contribution of land use to the interannual variability of the land carbon cycle. *Nat. Commun.* **2020**, *11*, 3170. [CrossRef]
19. Dixon, R.K.; Solomon, A.M.; Brown, S.; Houghton, R.A.; Trexier, M.C.; Wisniewski, J. Carbon pools and flux of global forest ecosystems. *Science* **1994**, *263*, 185–190. [CrossRef]
20. Piao, S.; Fang, J.; Ciais, P.; Peylin, P.; Huang, Y.; Sitch, S.; Wang, T. The carbon balance of terrestrial ecosystems in China. *Nature* **2009**, *458*, 1009–1013. [CrossRef]
21. Houghton, R.A. Revised estimates of the annual net flux of carbon to the atmosphere from changes in land use and land management 1850–2000. *Tellus B Chem. Phys. Meteorol.* **2002**, *55*, 378. [CrossRef]
22. Elvidge, C.D.; Baugh, K.E.; Dietz, J.B.; Bland, T.; Sutton, P.C.; Kroehl, H.W. Radiance Calibration of DMSP-OLS Low-Light Imaging Data of Human Settlements. *Remote Sens. Environ.* **1999**, *68*, 77–88. [CrossRef]
23. Wang, T.; Zhang, Y.; Yue, C.; Wang, Y.; Wang, X.; Lyu, G.; Wei, J.; Yang, H.; Piao, S. Progress and challenges in remotely sensed terrestrial carbon fluxes. *Geo-Spat. Inf. Sci.* **2025**, *28*, 1–21. [CrossRef]
24. Houghton, R.A.; House, J.I.; Pongratz, J.; van der Werf, G.R.; DeFries, R.S.; Hansen, M.C.; Le Quéré, C.; Ramankutty, N. Carbon emissions from land use and land-cover change. *Biogeosciences* **2012**, *9*, 5125–5142. [CrossRef]
25. Houghton, R.A. The emissions of carbon from deforestation and degradation in the tropics: Past trends and future potential. *Carbon Manag.* **2013**, *4*, 539–546. [CrossRef]
26. Parton, W.J.; Holland, E.A.; Del Grosso, S.J.; Hartman, M.D.; Martin, R.E.; Mosier, A.R.; Ojima, D.S.; Schimel, D.S. Generalized model for NO_x and N_2O emissions from soils. *J. Geophys. Res.* **2001**, *106*, 17403–17419. [CrossRef]
27. van der Werf, G.R.; Randerson, J.T.; Collatz, G.J.; Giglio, L. Carbon emissions from fires in tropical and subtropical ecosystems. *Glob. Change Biol.* **2003**, *9*, 547–562. [CrossRef]
28. Sullivan, M.J.P.; Talbot, J.; Lewis, S.L.; Phillips, O.L.; Qie, L.; Begne, S.K.; Chave, J.; Cuni-Sanchez, A.; Hubau, W.; Lopez-Gonzalez, G.; et al. Diversity and carbon storage across the tropical forest biome. *Sci. Rep.* **2017**, *7*, 39102. [CrossRef]
29. Matiza, C.; Mutanga, O.; Peerbhay, K.; Odindi, J.; Lottering, R. A systematic review of remote sensing and machine learning approaches for accurate carbon storage estimation in natural forests. *South. For. A J. For. Sci.* **2023**, *85*, 123–141. [CrossRef]
30. Sharma, S.; Dhal, S.; Rout, T.; Acharya, B.S. Drones and machine learning for estimating forest carbon storage. *Carbon Res.* **2022**, *1*, 21. [CrossRef]
31. Schwalm, C.R.; Williams, C.A.; Schaefer, K. Carbon consequences of global hydrologic change, 1948–2009. *J. Geophys. Res.* **2011**, *116*, 1–7. [CrossRef]
32. Wei, W.; Bao, Y.; Wang, Z.; Chen, X.; Luo, Q.; Mo, Y. Response of habitat quality to urban spatial morphological structure in multi-mountainous city. *Ecol. Indic.* **2023**, *146*, 109877. [CrossRef]
33. Wu, A.; Wang, Z. Multi-scenario simulation and carbon storage assessment of land use in a multi-mountainous city. *Land Use Policy* **2025**, *153*, 107529. [CrossRef]

34. Chen, J.; Yang, J.; Lu, D.; Wang, F.; Yang, D.; He, T. Evaluation, Coordination Relationship, and Obstacle Factor Analysis of Integrated Urban–Rural Development in Counties of Wuling Mountain Area. *Sustainability* **2025**, *17*, 10010. [CrossRef]
35. Lu, D.; Yang, D.; Li, M.; Lu, T.; Han, C. Nonlinear Mechanisms of $PM_{2.5}$ and O_3 Response to 2D/3D Building and Green Space Patterns in Guiyang City, China. *Land* **2025**, *14*, 2257. [CrossRef]
36. Chen, X.; Wang, Z.; Bao, Y. Cool Island effects of urban remnant natural mountains for cooling communities: A case study of Guiyang, China. *Sustain. Cities Soc.* **2021**, *71*, 102983. [CrossRef]
37. Kong, N.; Wang, Z. Response of Plant Diversity of Urban Remnant Mountains to Surrounding Urban Spatial Morphology: A Case Study in Guiyang of Guizhou Province, China. *Urban Ecosyst.* **2021**, *25*, 437–452. [CrossRef]
38. Luo, Q.; Bao, Y.; Wang, Z.; Chen, X. Potential recreation service efficiency of urban remnant mountain wilderness: A case study of Yunyan District of Guiyang city, China. *Ecol. Indic.* **2022**, *141*, 109081. [CrossRef]
39. Ghosh, S.; Dinda, S.; Chatterjee, N.D.; Dutta, S.; Bera, D. Spatial-explicit carbon emission-sequestration balance estimation and evaluation of emission susceptible zones in an Eastern Himalayan city using Pressure-Sensitivity-Resilience framework: An approach towards achieving low carbon cities. *J. Clean. Prod.* **2022**, *336*, 130417. [CrossRef]
40. Lin, Q.; Zhang, L.; Qiu, B.; Zhao, Y.; Wei, C. Spatiotemporal Analysis of Land Use Patterns on Carbon Emissions in China. *Land* **2021**, *10*, 141. [CrossRef]
41. Wang, Q.-F.; Jin, Y.-H.; Sun, P.; Xiao, Y.; Chen, Z.-H.; Lu, Z.-R.; Liang, H.-S. A Method for Fine Mapping of Carbon Emissions from Regional Land Use Change and Its Application. *Huan Jing Ke Xue* **2024**, *45*, 5060–5068. [CrossRef]
42. Jiang, X.; Chu, X.; Yang, X.; Jiang, P.; Zhu, J.; Cai, Z.; Yu, S. Spatiotemporal Dynamics of Land Use Carbon Balance and Its Response to Urbanization: A Case of the Yangtze River Economic Belt. *Land* **2025**, *14*, 41. [CrossRef]
43. Rong, T.; Zhang, P.; Jing, W.; Zhang, Y.; Li, Y.; Yang, D.; Yang, J.; Chang, H.; Ge, L. Carbon Dioxide Emissions and Their Driving Forces of Land Use Change Based on Economic Contributive Coefficient (ECC) and Ecological Support Coefficient (ESC) in the Lower Yellow River Region (1995–2018). *Energies* **2020**, *13*, 2600. [CrossRef]
44. Cui, Y.; Li, L.; Chen, L.; Zhang, Y.; Cheng, L.; Zhou, X.; Yang, X. Land-Use Carbon Emissions Estimation for the Yangtze River Delta Urban Agglomeration Using 1994–2016 Landsat Image Data. *Remote Sens.* **2018**, *10*, 1334. [CrossRef]
45. Guo, A.; Niu, L.; Liu, P.; Li, Y. Carbon emission from land use in urban agglomeration of the Yellow River basin. *Econ. Geogr.* **2023**, *43*, 172–178. [CrossRef]
46. Zhang, Z.; Hou, Y.; Sun, H. Calculation of carbon emissions and the difference of low-carbon development efficiency on city territorial space. *J. Nat. Resour.* **2023**, *38*, 1464. [CrossRef]
47. Wang, J.; Wei, J.; Zhang, W.; Liu, Z.; Du, X.; Liu, W.; Pan, K. High-resolution temporal and spatial evolution of carbon emissions from building operations in Beijing. *J. Clean. Prod.* **2022**, *376*, 134272. [CrossRef]
48. Huisingh, D.; Zhang, Z.; Moore, J.C.; Qiao, Q.; Li, Q. Recent advances in carbon emissions reduction: Policies, technologies, monitoring, assessment and modeling. *J. Clean. Prod.* **2015**, *103*, 1–12. [CrossRef]
49. Liang, Y.; Niu, D.; Wang, H.; Chen, H. Assessment Analysis and Forecasting for Security Early Warning of Energy Consumption Carbon Emissions in Hebei Province, China. *Energies* **2017**, *10*, 391. [CrossRef]
50. Han, S.; Zhu, M.; Liu, H.; Song, Y. Research on Carbon Emissions Monitoring and Early Warning System: Analysis Based on the Provincial Panel Data of China. *Ecol. Econ.* **2022**, *38*, 21–27.
51. Lv, T.; Hu, H.; Zhang, X.; Xie, H.; Wang, L.; Fu, S. Spatial spillover effects of urbanization on carbon emissions in the Yangtze River Delta urban agglomeration, China. *Environ. Sci. Pollut. Res. Int.* **2022**, *29*, 33920–33934. [CrossRef]
52. Chen, J.; Gao, M.; Cheng, S.; Liu, X.; Hou, W.; Song, M.; Li, D.; Fan, W. China's city-level carbon emissions during 1992–2017 based on the inter-calibration of nighttime light data. *Sci. Rep.* **2021**, *11*, 3323. [CrossRef]
53. Zhang, X.; Wu, J.; Peng, J.; Cao, Q. The Uncertainty of Nighttime Light Data in Estimating Carbon Dioxide Emissions in China: A Comparison between DMSP-OLS and NPP-VIIRS. *Remote Sens.* **2017**, *9*, 797. [CrossRef]
54. Liu, L.Y.; Chen, L.F.; Liu, Y.; Yang, D.X.; Zhang, X.Y.; Lu, N.M.; Ju, W.M.; Jiang, F.; Yin, Z.S.; Liu, G.H.; et al. Satellite remote sensing for global stocktaking: Methods, progress and perspectives. *Natl. Remote Sens. Bull.* **2022**, *26*, 243–267. [CrossRef]

Disclaimer/Publisher's Note: The statements, opinions and data contained in all publications are solely those of the individual author(s) and contributor(s) and not of MDPI and/or the editor(s). MDPI and/or the editor(s) disclaim responsibility for any injury to people or property resulting from any ideas, methods, instructions or products referred to in the content.